

# Numerical Simulation of the Fast Processes in a Vacuum Electrical Discharge

I. V. Uimanov

*Institute of Electrophysics of RAS  
Russia*

## 1. Introduction

A vacuum electrical discharge goes over three stages: breakdown, a spark, and an arc (Mesyats, 2000). The arc stage is the most mysterious form of the vacuum discharge. Since the discovery of the vacuum arc, the nature of the physical processes responsible for its operation has been debatable. The situation is paradoxical: vacuum arcs are widely used in various technologies, namely, in high-current switches, vacuum-arc melting and welding, plasma-assisted ion deposition, coating deposition, ion implantation, etc., and, at the same time, there is no commonly accepted idea about the mechanism of a vacuum discharge. Besides, the pulsed vacuum discharge is now the basic phenomenon harnessed in pulsed power and electronics. Pulsed electron beams are used in various fields, in particular for the production of braking x-ray pulses (radiography of fast processes, nondestructive testing), for the investigation of plasma-beam interactions, and for the production of superpower pulsed microwaves (heating of thermonuclear plasmas, long-range radar). It should be noted that practically in all cases, the spark (explosive electron emission (EEE)) stage of a vacuum discharge is used for the production of electron beams, and explosive-emission cathodes today have no alternative as components of pulsed high-current electrophysical devices. By the present time, the pulse range with the duration of processes as short as a few nanoseconds has been mastered rather well. Note that a way of increasing the power dissipated in the load of a high-voltage generator at a given stored energy is to reduce the voltage pulse duration. Therefore, in the recent years significant efforts have been made to develop high-current pulsed devices operating in the subnanosecond and picosecond ranges of voltage pulse durations (Mesyats & Yalandin, 2005).

It has been revealed in numerous experiments that the fundamental properties of a vacuum discharge are entirely determined by the processes that occur in a small brightly luminous region at the cathode through which the current transfer between the cathode and the electrode gap is realized. This region is termed the cathode spot and it includes the active part of the cathode surface heated to temperatures far above the melting point and the cathode plasma generated as a result of the material transfer from the active part of the cathode in the vacuum gap.

The existing theoretical models of the cathode spot phenomena can be conventionally subdivided into two groups in relation to the mechanism of formation of the conducting medium in vacuum. The models of the first group are based on the assumption of thermal

evaporation of the cathode material (Boxman et al., 1995; Lyubimov & Rakhovskii, 1978). However, this approach does not allow one to interpret well-known experimental data. The second-group models suppose explosive generation of the cathode plasma as a result of intense heating of microregions of the cathode surface. Theoretical ideas about explosive generation of the cathode plasma have been formulated most adequately in the ecton model of the cathode spot (Mesyats, 2000). In terms of this concept, all the three stages of a vacuum discharge appear explicable on the basis of natural origins. Breakdown and the so-called prebreakdown phenomena constitute a process of energy concentration in a microvolume at the cathode surface. Once the specific energy stored in a microvolume has become higher than a certain limiting value, an explosion begins and the breakdown stage is completed. The beginning of an explosion and the appearance of EEE is the onset of the spark stage of the discharge. The spark stage involves continuous regeneration of microexplosions by the plasma and liquid-metal jets produced by preceding microexplosions. The spark stage naturally goes over into the arc stage as the cathode and anode plasmas come together and the current rise rate decreases. However, the quantitative description of the cathode phenomena in the context of this model has yet been made only based on simplified estimating notions.

Thus, despite the significant advance in the study of some characteristic of cathode spots, a commonly accepted model of the cathode spot of a vacuum discharge yet does not exist. This is related, first, to the problems of experimental diagnostics of cathode spots in view of the extremely small time and space scales of the cathode spot phenomena and of their fast and chaotic motion over the cathode surface. Therefore, numerical simulation still remains practically a single method allowing one to determine the discharge parameters taking into account their space and time dependences.

The present paper is devoted to a numerical simulation of the prebreakdown phenomena in the cathode that take place on the initiation of an electrical discharge in a vacuum gap by application of a pulsed high voltage to the electrodes and also to a simulation of the processes initiating explosive emission centers on the cathode upon its interaction with the cathode spot plasma. Both processes in fact determine the mechanism of generation of the conducting medium in the electrode gap; therefore, to study them is of importance for constructing a self-consistent model of a vacuum discharge. In the first case, attention is mostly given to the subnanosecond range of voltage pulse durations. From the practical viewpoint, knowledge of the phenomena occurring on the nanosecond scale would be helpful in analyzing the efficiency of operation of explosive emission cathodes in a picosecond pulse mode. As for the second problem, the plasma-cathode interaction is the dominant process in the mechanism of self-sustainment of a vacuum discharge.

It is well known that under the conditions of high vacuum and pure electrodes, electrical discharge in vacuum is initiated by the current of field electron emission (FEE). According to the criterion for pulsed breakdown (Mesyats, 2000), to attain subnanosecond time delays to the explosion of a cathode microprotrusion, a field emission current density over  $10^9$  A/cm<sup>2</sup> is necessary. It is obvious that at these high field emission current densities, the screening of the electric field at the cathode surface by the space charge of emitted electrons substantially affects the field strength. It has even been speculated that this effect can have grave consequences: it will be impossible to produce current densities which would be high enough to achieve subnanosecond explosion delay times. The second section of proposed work is devoted to a study of the effect of the space charge of emitted electrons on the

electric field strength near the surface of the field emission emitters and a point microprotrusion on a metal cathode by using a two-dimensional axisymmetric problem statement. Based on the particle-in-cell (PIC) method, a model has been developed and self-consistent calculations of the electric field strength at the cathode and its field emission characteristics has been performed. In the third section a two-dimensional, two-temperature model has been developed to describe the prebreakdown phenomena in a cathode microprotrusion at picosecond and subnanosecond durations of the applied voltage pulse. The simulation procedure includes a particle-in-cell simulation to calculate the self-consistent electric field at the cathode surface and the field-emission characteristics of the cathode. In the fourth section a two-dimensional nonstationary model of the initiation of new explosive centers beneath the plasma of a vacuum arc cathode spot has been developed. In terms of this model, the plasma density and electron temperature that determine the ion current from the plasma to the microprotrusion and the microprotrusion geometry were treated as the external parameters of the problem. The process of heating of a cathode surface microprotrusion, for which both a surface irregularity resulting from the development of a preceding crater and the edge of an active crater, which may be a liquid-metal jet, can be considered, has been simulated numerically.

## **2. PIC simulation of the screening of the electric field at the cathode surface under intense field emission**

The fact that the space charge (SC) of the electrons emitted from a metal affects the metal field-emission characteristics is now beyond question. The problem was first raised (Stern et al., 1929) shortly after the creation of the Fowler-Nordheim (F-N) theory (Fowler & Nordheim, 1928; Nordheim, 1929). However, it became urgent once Dyke and Trolan (Dyke & Trolan, 1953) had revealed an appreciable deviation from the F-N law at current densities  $j > 5 \cdot 10^6$  A/cm<sup>2</sup>, which showed up in a weaker dependence of the emission current on the applied potential difference. The authors (Dyke & Trolan, 1953) accounted for the nonlinearity of the current-voltage characteristics (CVCs) by the reduction of the electric field at the cathode surface due to the presence of a space charge of emitted electrons. In the subsequent work (Barbour et al., 1963), they proposed a model of an equivalent planar diode (EPD). This model, with properly chosen parameters, allowed one not only to describe qualitatively the deviation of a CVC toward the lower currents due to the SC effect, but also to obtain a reasonable agreement with experimental data. Therefore, for a long time it was considered established, both experimentally and theoretically, that the field-emission current density is limited to a level of  $\sim 10^7$  A/cm<sup>2</sup> by the emission beam SC.

However, the problem appears to be not conclusively solved if field emission studies involve nanostructured surfaces and emitters where the emission occurs from nanometer objects. Investigations of the FEE from specially produced nanometer protrusions (Pavlov et al., 1975; Fursey et al., 1998) have shown that linear CVCs can be observed for current densities up to  $\sim 10^{10}$  A/cm<sup>2</sup>, which are three orders of magnitude greater than those characteristic of conventional metal emitters with a tip radius of  $\sim 10^{-5}$ – $10^{-4}$  cm. Thus, though the current density is undoubtedly the determining quantity in the formation of the SC of a field emission beam, it is not the only factor responsible for the substantial effect of the SC on FEE. This necessitates a more rigorous consideration of this problem by invoking models that would describe the formation and spatial relaxation of the SC of an emission beam in a

more realistic geometry than this is possible in the context of the EPD model. This problem is also important in view of considerable advances in the study of field emission properties of various nanostructured surfaces, carbon nanotubes (Guillorn et al., 2004), dielectric and semiconductor matrices with conducting inclusions (Forbes, 2001), and Spindt cathodes (Spindt, 1968). In high current electronics, these investigations are of interest from the viewpoint of evaluating the efficiency of explosive-emission cathodes for the production of picosecond electron beams, because to initiate FEE within such short times, rather high FEE current densities ( $\sim 10^{10}$  A/cm<sup>2</sup>) are necessary (Mesyats & Uimanov, 2008).

Theoretically, the investigation of the effect of the SC on FEE was practically limited to the solution of the one-dimensional Poisson equation for an EPD or for a spherical diode (ESD) (see (Shrednik, 1974) and the cited literature). The one-dimensional approach naturally used in the previous work considerably moderates computational difficulties, but even in these cases, numerical calculations are required. This in the main is due to the nonlinearity of the F-N relation, which is used as a boundary condition in the problem statement. However, the applicability of a one-dimensional approximation to the actual geometry of a point-cathode vacuum diode has not been yet strictly substantiated. The only argument in favor of the usability of the EPD model advanced by the authors of Ref. (Barbour et al., 1963) is the estimate of the parameter of spatial localization of the SC near the emission surface. A critical analysis of the use of the EPD and ESD models for the description of the effect of the emission beam SC can be found elsewhere (Pavlov, 2004). The EPD model was adapted to describe the effect of the SC of emitted electrons on the field strength and current density distributions over the emitter surface (Shkuratov et al., 1960 (1995)). A similar approach was used with the ESD model (Batrakov et al., 1999). It has been shown (Shkuratov et al., 1960 (1995); Batrakov et al., 1999) that the SC of an emission beam not only efficiently screens the field at the cathode, but also significantly changes its distribution over the surface. However, it remains unclear for today whether the use of these quasi-two-dimensional approaches, offered largely *ad hoc*, is adequate. It should be noted that the particle-in-cell method was first used for solving the problem under consideration in Ref. (Batrakov et al., 1999). However, in our opinion, its capabilities, as applied to solving problems of this type, could not be efficiently used in spherical one-dimensional calculations. We were the first to make an attempt to solve the problem on the effect of the SC of emitted electrons on the electric field strength and on the CVC of the vacuum gap in a two-dimensional axially symmetric statement (Uimanov, 2008; Uimanov, 2010). We used the weighed-particle-in-cell method to simulate the self-consistent field-emission beam emitted by a microprotrusion on a macropoint cathode. The results obtained with the model developed have allowed us to analyze both the details of the screening phenomenon and the probable values of fields and current densities for the cathode protrusions of micrometer and submicrometer dimensions. In the study we present here, we used this model to investigate the external field screening not only for macropoint cathodes with microprotrusions, but also for classical point field emitters over a rather wide range of the geometric parameters of the cathode.

## 2.1 Problem statement and task geometry

Figure 1 presents the model geometry of the problem. As a whole it is the coaxial diode with distance the cathode - anode 1 cm. The cathode is the metal needle with the tip radius  $r_c$ . On the surface of the cathode there is a microprotrusion of height  $h_m$ , tip radius  $r_m$  and the half-angle of the conical part  $\Theta$ .

This cathode geometry takes into account the two-factor field enhancement at the microprotrusion surface which is typical of the electrode systems that were used in the experimental studies of EEE performed by now on the subnanosecond scale.

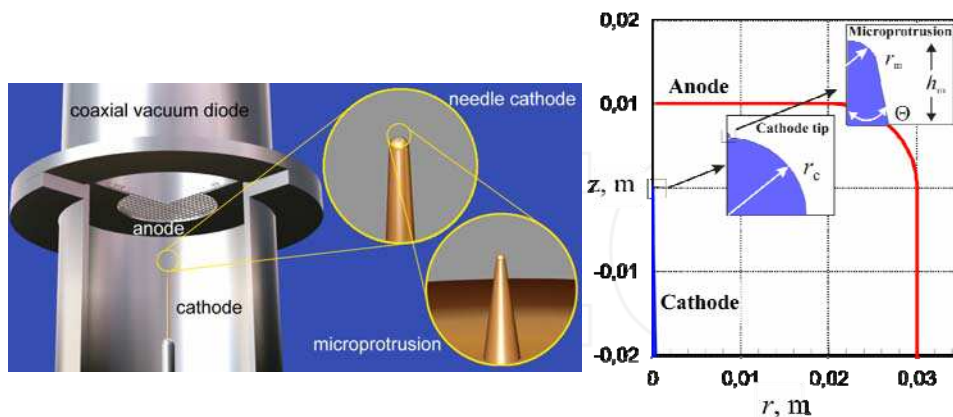


Fig. 1. Task geometry. Calculated parameters:  $r_c = 50 \mu\text{m}$ ,  $h_m = 5 \mu\text{m}$ ,  $r_m = 0.1 \mu\text{m}$ ,  $\Theta = 10^\circ$

Approximately the factor of electric field enhancement for such geometry is  $\beta_{\text{tot}} = \beta_c \beta_m$ , where  $\beta_c$  is the factor of electric field enhancement of the point cathode,  $\beta_m$  is the factor of the microprotrusion. The large difference in characteristic scales of the microprotrusion and all diode is one of the main difficulties of the task.

## 2.2 Mathematical model

The electric field potential  $u$  in the diode is calculated with the Poisson equation:

$$\begin{aligned} \Delta u(r, z) &= -4\pi\rho(r, z) \\ \varphi|_{\text{cathode}} &= -U, \quad \varphi|_{\text{anode}} = 0' \end{aligned} \quad (1)$$

where  $\rho$  is the space charge density of emitted electrons, which was found by the particle-in-cell method (Hockney & Eastwood, 1988; Birdsall & Langdon, 1985). This equation was solved by a set up method up to decision of a stationary solution at the curvilinear boundary-fitted grid (see Fig. 2). In our electrostatic PIC simulation, each computer particle is a “superparticle” which represents some number of real electrons. The charge of these “superparticles” is not constant and it is defined by expression  $q_p = j_{\text{em}} \Delta S_i \Delta t$ , where  $j_{\text{em}}$  is the FEE current density,  $\Delta S_i$  is the elementary area of the emission surface,  $\Delta t$  is time step. The particles start at the cathode microprotrusion, as a result of the FEE process. The particles are then followed, one after the other, during successive time steps. Their trajectory is calculated by Newton’s laws

$$\begin{aligned} z &= z_0 + v_z^0 \Delta t, & r &= r_0 + v_r^0 \Delta t, \\ v_z &= v_z^0 + \frac{e}{m} E_z(r, z) \Delta t, & v_r &= v_r^0 + \frac{e}{m} E_r(r, z) \Delta t, \end{aligned} \quad (2)$$

where  $z_0, r_0$  and  $z, r$  are the position coordinates before and after  $\Delta t$ ,  $v_z^0, v_r^0$  and  $v_z, v_r$  are the velocities before and after  $\Delta t$ ,  $E_z = -du/dz$  and  $E_r = -du/dr$  are the axial and radial electric field,  $e$  and  $m$  are the electron charge and mass, respectively.

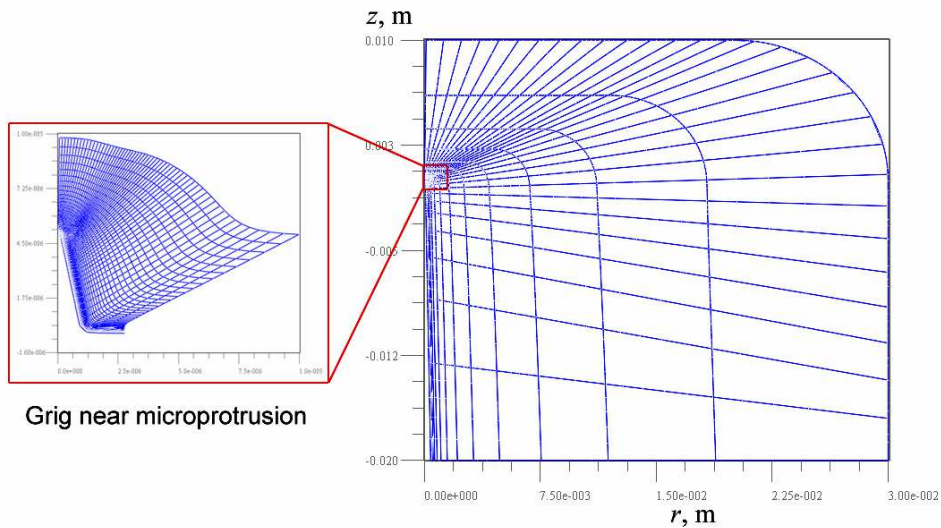


Fig. 2. Discrete representation of the model geometry with a boundary-fitted grid

In a typical electrostatic PIC simulation, for each time step:

1. The charge density  $\rho(r, z)$  is obtained by a bilinear weighting of the particles to the spatial curvilinear grid (Seldner & Westermann, 1988).
2.  $\rho(r, z)$  is used in Poisson's equation to solve for the electric field  $\vec{E} = -\vec{\nabla}u$ .
3.  $E_z$  and  $E_r$  are bilinearly weighted back to each particle position in order to determine the force on each particle.
4. The Newton equations of motion (2) are used to advance the particles to new positions and velocities.
5. The boundaries are checked, and out of bounds particles are removed.

The FEE current density  $j_{em}$  was assumed to depend on the self-consistent electric field at the microprotrusion surface in accordance with Miller-Good (MG) approximation (Modinos, 1984):

$$j_{em} = \frac{4\pi me}{h^3} \int_0^\infty d\varepsilon \int_0^\varepsilon d\varepsilon_n f_{FD}(\varepsilon) D(E_{em}, \varepsilon_n), \quad (3)$$

where  $D(E_{em}, \varepsilon_n)$  is the transparency of the potential barrier,  $E_{em}$  is the electric field at the cathode,  $\varepsilon = (\hbar k)^2 / 2m$  is the electron energy in the metal,  $\varepsilon_n = (\hbar k_n)^2 / 2m$  is the energy component of an electron in the metal which is "normal to the emission boundary",  $\hbar$  ( $\hbar = h / 2\pi$ ) is the Plank constant. We assume that  $f_{FD}(\varepsilon) = \{1 + \exp((\varepsilon - \varepsilon_F) / k_B T_e)\}^{-1}$  is the

equilibrium Fermi-Dirac function, where  $\varepsilon_F$  is the Fermi energy,  $k_B$  is Boltzmann's constant,  $T_e = 300^\circ\text{K}$  is the electron temperature.

Within the framework of the MG approximation, the expression for the transmission factor of a barrier has the form (Modinos, 1984):

$$D(E_{\text{em}}, \varepsilon_n) = \begin{cases} [1 + \exp(Q(E_{\text{em}}, \varepsilon_n))]^{-1}, & \varepsilon_n < \varepsilon_L, \\ 1, & \varepsilon_n > \varepsilon_L, \end{cases} \quad (4)$$

$$Q(E_{\text{em}}, \varepsilon_n) = \frac{4\sqrt{2}}{3} \left( \frac{m^2 e^5}{\hbar^4 E_{\text{em}}} \right)^{1/4} y^{-3/2} v(y), \quad (5)$$

$$y = \sqrt{e^3 E_{\text{em}}} / |\varepsilon_F + \varphi - \varepsilon_n|, \quad (6)$$

where  $\varepsilon_L = \varepsilon_F + \varphi - 1/\sqrt{2} \sqrt{e^3 E_{\text{em}}}$ ,  $\varphi$  is work function,  $v(y)$  is a function, which is defined through elliptic integrals (Modinos, 1984). The rigorous boundary condition on the cathode surface (3) is another factor that substantially complicates the solution and restricts the choice of the solution technique.

### 2.3 Results

PIC simulations were performed for a copper cathode in the voltage range  $U = 5\text{--}500$  kV. The results of the numerical calculation of the FEE characteristics are presented in Fig. 3 whose geometric parameters are given in Fig. 1. Figure 3 a) gives the results of computation for the maximal FEE current density on the microprotrusion tip. Figure 3 b) presents the results of the PIC simulations of the total FEE current.

Figure 4 presents the distributions of the electric field strength a) and field emission current density b) over the microprotrusion surface at different voltages. From Fig. 4 it can be seen that at  $j_{\text{em}} > 10^7$  A/cm<sup>2</sup> the space charge substantially affects both the magnitude of the field and its distribution over the surface. Note that if the space charge would not been taken into account, the field distribution in Fig. 4 a) would remain constant. Analyzing the curves in Fig. 4 b), it can be noted that the screening effect results in increase of the "effective emission surface".

The results of the numerical calculation of the screening effect of the external electric field by the FEE electron space charge are illustrated in Fig. 5. and Fig. 6. The results obtained show that in the range of high FEE currents ( $j_{\text{em}} > 10^9$  A/cm<sup>2</sup>) the self-consistent field strength is in fact an order of magnitude lower than its geometric value. Figure 6 presents the respective curves for microprotrusions with different tip radii. From this figure it can be seen that a decrease in tip radius decreases the screening efficiency. This effect is essentially two-dimensional in character. Because the space charge is localized within  $\sim 10^{-7}$  m of the emitting surface, the smaller  $r_{\text{nv}}$ , the lesser is portion of the space charge that participates in the screening of the external field at the microprotrusion tip.

For comparison, the dashed curves in Fig. 3, a) and in Fig. 5, a represent the results that we have obtained by using a quasi-two-dimensional EPD model (Barbour et al., 1963). Analyzing the curves obtained, it can be noted that this model overestimates influence of the SC of the FEE electrons.

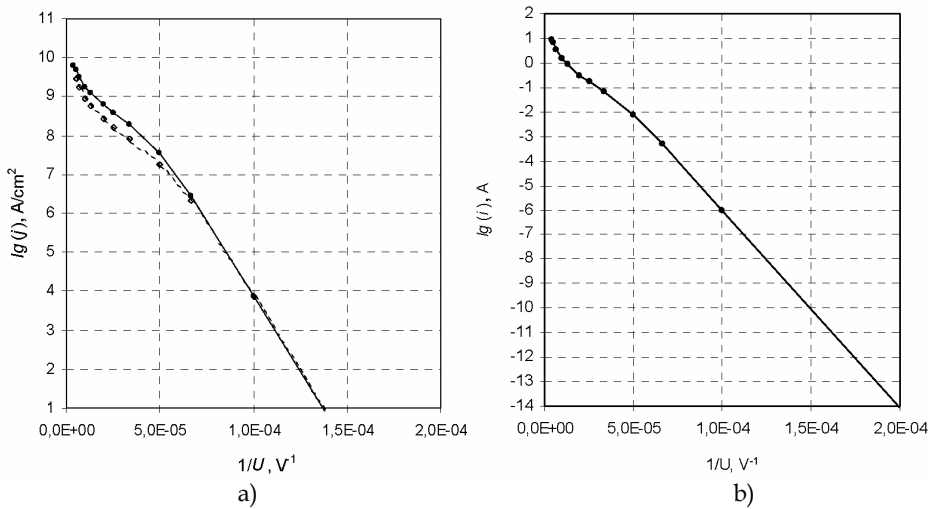


Fig. 3. Calculated current-voltage characteristics for Cu cathode with work function 4.4 eV: a) the FEE current density on the microprotrusion tip ( $r = 0$ ): 1 - PIC simulations, 2 - numerical calculations within the framework of the EPD model (Barbour et al., 1963); b) PIC simulations of the total FEE current

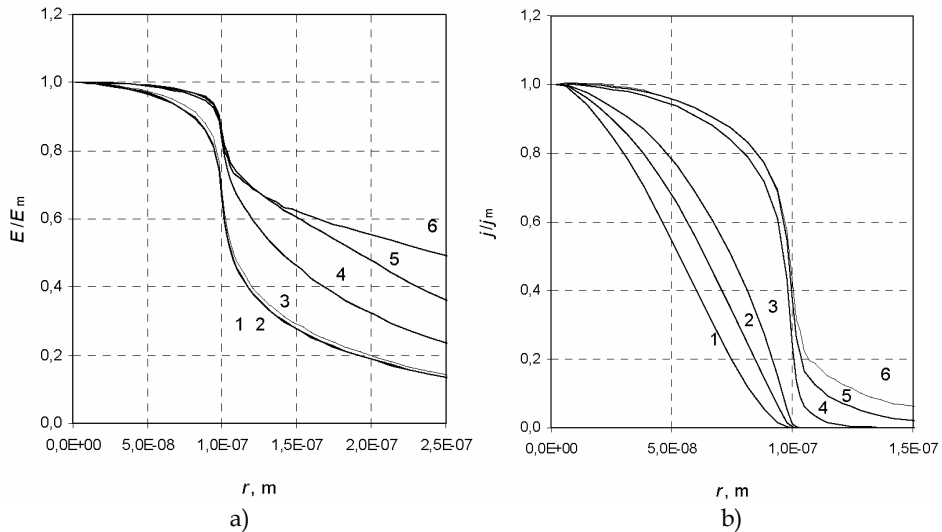


Fig. 4. Electric field strength a) and field emission current density b) distributions over the microprotrusion surface at different voltages (Geometric parameters are given in Fig. 1.): 1 - 5 kV,  $E_m = 1.9 \cdot 10^7$  V/cm,  $j_m = 1.2 \cdot 10^{-4}$  A/cm²; 2 - 15 kV,  $E_m = 5.6 \cdot 10^7$  V/cm,  $j_m = 2.7 \cdot 10^6$  A/cm²; 3 - 20 kV,  $E_m = 7.1 \cdot 10^7$  V/cm,  $j_m = 3.4 \cdot 10^7$  A/cm²; 4 - 50 kV,  $E_m = 10^8$  V/cm,  $j_m = 6 \cdot 10^8$  A/cm²; 5 - 100 kV,  $E_m = 1.2 \cdot 10^8$  V/cm,  $j_m = 1.8 \cdot 10^9$  A/cm²; 6 - 250 kV,  $E_m = 1.5 \cdot 10^8$  V/cm,  $j_m = 6.2 \cdot 10^9$  A/cm²



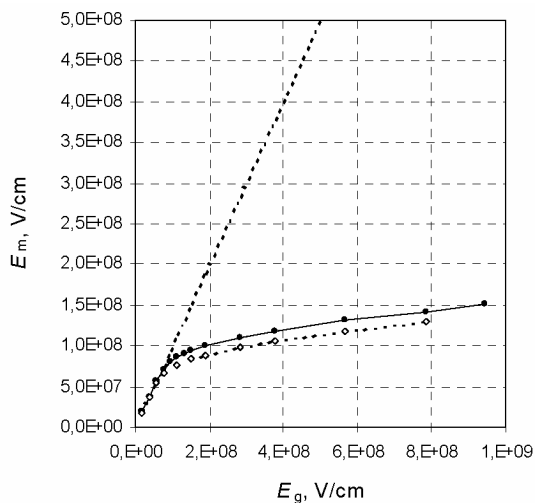


Fig. 5. SC-limited self-consistent electric field at the microprotrusion tip versus geometric field (without taking into account the space charge effect): 1 – geometric field, 2 – PIC simulations, 3 – EPD model (Barbour et al., 1963). Calculated parameters:  $\varphi = 4.4$  eV,  $r_c = 50$   $\mu\text{m}$ ,  $h_m = 5$   $\mu\text{m}$ ,  $r_m = 0.1$   $\mu\text{m}$ ,  $\theta = 10^\circ$

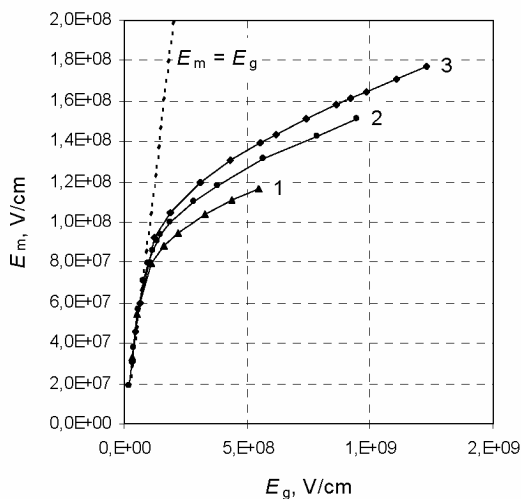


Fig. 6. SC-limited self-consistent electric field at the microprotrusion tip versus geometric field for microprotrusions with different tip radii: 1 –  $r_m = 0.5$   $\mu\text{m}$ , 2 –  $r_m = 0.1$   $\mu\text{m}$ , 3 –  $r_m = 0.05$   $\mu\text{m}$ . Calculated parameters:  $\varphi = 4.4$  eV,  $r_c = 50$   $\mu\text{m}$ ,  $h_m = 5$   $\mu\text{m}$ ,  $\theta = 10^\circ$

## 2.4 The dimensional effect of the space charge of the emitted electrons on the strength of the self-consistent electric field at the cathode surface

The investigations were performed with the use of above model. The model covers both the trajectory part of the problem and the axially symmetric self-consistent solution of the Poisson equation for the electric field potential over the entire vacuum gap taking into account the SC of emitted electrons. The electron trajectories and the space charge of the emission beam are calculated by the particle-in-cell method using a scheme including macroparticles of varied charge and algorithms of particle coarsening. Coaxial electrode configurations with a point field emitter and the case of emission from a cathode protrusion (see Fig. 1), which are inherent in FEE and EEE investigations, were considered. In both cases, the axial cathode-anode separation was 1 cm. The Dyke model (Dyke et al., 1953) was used for an approximate description of the shape of the point field emitter (see Fig. 7). According to this model, the shape of an emitter prepared by electrolytic etching can be presented rather precisely by the equipotential surface of an electric field produced by a charged orthogonal cone with a sphere on its vertex. The equipotential surface and, hence, the shape of the emitter are specified by three parameters: the radius of the emitter tip,  $r_0$ , the radius of the kernel sphere,  $a$ , and the order of the Legendre polynomial,  $n$ . If the anode is also shaped as an equipotential surface, the solution of the Laplace equation for a system of this configuration is well known (Dyke et al., 1953). Though the field is calculated numerically in our model, the use of this approach allows one to control the procedure of construction of an essentially nonuniform curvilinear computational grid by comparing the accuracy of the numerical solution of the Laplace equation with that of the analytic solution.

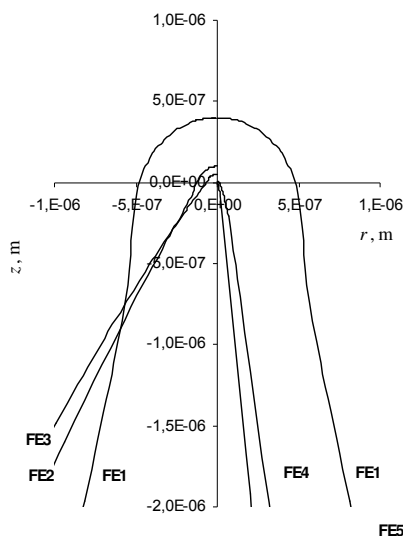


Fig. 7. The shape of model field emitters

The resulting grid is also used for solving the Poisson equation. The parameters of the field emitters that were used in the calculations are given in Table 1. The last column presents the  $\beta_0$  factor of the emitter, which is calculated numerically from the relation  $\beta_0 = E_0 / U$ , where  $E_0$  is the field at the tip and  $U$  is the cathode-anode potential difference.

N	$r_0 \cdot 10^{-5}, \text{ cm}$	$a \cdot 10^{-5}, \text{ cm}$	$n$	$\beta_0, \text{ cm}^{-1}$
FE1	4.0	1.235	0.1	4613
FE2	1.0	0.524	0.2416	4618
FE3	0.5	0.25	0.2835	4599
FE4	0.1	0.02	0.1	$8.0 \cdot 10^4$
FE5	0.01	0.002	0.1	$5.7 \cdot 10^5$

Table 1. Parameters of field emitters

The field strength on the cathode tip calculated as a function of its “geometric” value  $E_g$  (Laplace field not taking into account the SC of emitted electrons) and the CVC of the vacuum gap calculated in terms of F-N coordinates for a set of emitters (FE1 through FE3) are shown in Fig. 8 and in Fig. 9, respectively. The emitters of this set are characterized by the same  $\beta_0$ . The data of the respective calculations for emitters FE4 through FE6 having the same cone angle are presented in Fig. 10 and in Fig. 11.

The results obtained suggest that the efficiency of the field screening by the SC of the emission beam depends, in the main, on the emitter radius (linear dimension of the emission area). The smaller the emitter radius, the lower the degree of weakening of the external field at the cathode by the SC of emitted electrons. It should be stressed that this refers both to point emitters and to cathodes with a protrusion. This dimensional effect shows up in the CVC as an increase in current density  $j_c$  at which the deviation from the linear F-N characteristic is observed. As can be seen from Fig. 9 and Fig. 11, as the emitter radius is decreased from  $4 \cdot 10^{-5}$  to  $10^{-7}$  cm,  $j_c$  increases approximately by two orders of magnitude, reaching  $\sim 10^9$  A/cm<sup>2</sup>. The results obtained agree with experimental data for FEE from nanometer protrusions (Pavlov et al., 1975; Fursey et al., 1998).

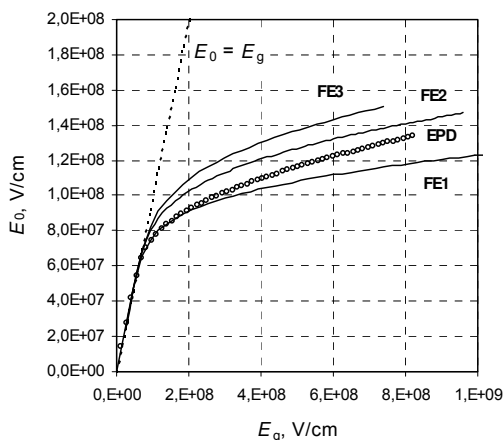


Fig. 8. The field strength at the emitter tip as a function of its geometric value for a set of emitters with the same  $\beta_0$

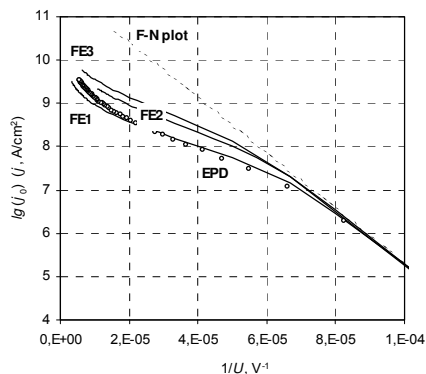


Fig. 9. The FEE current density as a function of the applied voltage for a set of emitters with the same  $\beta_0$

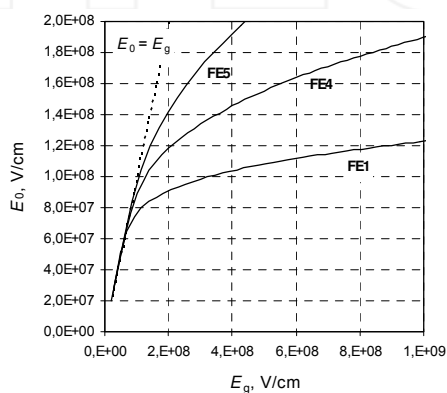


Fig. 10. The field strength at the emitter tip as a function of its geometric value for a set of emitters with the same cone angle

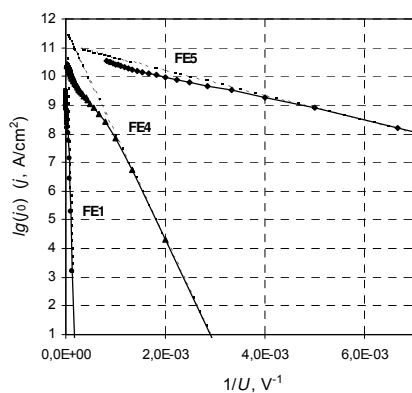


Fig. 11. The FEE current density as a function of the applied voltage for a set of emitters with the same cone angle

In Fig. 8 and Fig. 9, the round markers depict the characteristics under consideration calculated with the use of the EPD model for an emitter with  $\beta_0 = 4.6 \cdot 10^3 \text{ cm}^{-1}$ . As can be seen from these figures, good agreement with our results is observed for emitter FE1 with radius  $r_0 = 4 \cdot 10^{-5} \text{ cm}$  up to  $j \sim 5 \cdot 10^8 \text{ A/cm}^2$ . Note that the experimental data used in Ref. (Barbour et al., 1963) for comparison were limited to current densities even an order of magnitude lower. However, the results for more intense emission and, especially, for emitters with a smaller radius substantially disagree. Moreover, as emitters FE1 through FE3 have the same parameter  $\beta_0$ , the use of the EPD model yields one solution for this set, notwithstanding that the emitter radius varies within an order of magnitude. Our results evidently show a dependence on emitter radius.

### 3. Numerical simulation of vacuum prebreakdown phenomena at subnanosecond pulse durations

Considerable advances have recently been achieved in the development of high-current pulsed devices operating on the subnanosecond scale (Mesyats & Yalandin, 2005). In devices of this type, the electron beam is generally produced with the use of an explosive-emission cathode. It should be noted that with the effective duration of the explosive emission process equal to several hundreds of picoseconds, the explosion delay time should be at least an order of magnitude shorter, namely, some tens or even a few picoseconds. It is well known that under the conditions of high vacuum and clean electrodes, explosive electron emission is initiated by the current of field electron emission (Mesyats, 2000). The question of the FEE properties of metals in strong electric fields still remains open from both the theoretical and the experimental viewpoints (Mesyats & Uimanov, 2006). According to the criterion for pulsed breakdown to occur (Mesyats, 2000), to attain picosecond explosion delay times calls for FEE current densities more than  $10^9$ – $10^{10} \text{ A/cm}^2$ . Investigations performed on the nanosecond scale have shown that at high FEE current densities the electric field strength at the cathode surface is strongly affected by the screening of the electric field with the space charge of emitted electrons (Mesyats, 2000). This is indicated by the deviation of the experimental current-voltage characteristic from the Fowler–Nordheim plot (straight line) in the range of high currents. It was even supposed (Batrakov et al., 1999) that the screening effect may have fatal consequences, so that essentially high current densities which are required to shorten the explosion delay time to picoseconds or even subnanoseconds could not be achieved.

The aim of this section of this work was to investigate the fast processes of heat release and heat transfer that occur in point-shaped microprotrusions of the vacuum-diode cathode within the rise time of a subnanosecond high-voltage pulse. To attain this goal, self-consistent calculations of the field emission characteristics (the current density and the Nottingham energy flux density) were performed taking into account the space charge of emitted electrons (see sec. 2). Since the characteristic times of the processes considered were close to the time of relaxation of the lattice temperature, a two-temperature formulation was used for the model. The current density distribution in a cathode microprotrusion was calculated in view of a finite time of penetration of the electromagnetic field into the conductor.

#### 3.1 Description of the model

Pre-explosive processes occurring on the nanosecond and, the more so, on the microsecond scale, were investigated experimentally and theoretically for rectangular voltage pulses. At

present, this approach can hardly be realized experimentally on the subnanosecond scale. In the experiments described in the available literature (Mesyats & Yalandin, 2005), the pulse shape was near-triangular rather than rectangular with the voltage on the linear section of the leading edge rising at  $\sim 10^{15}$  V/s. Therefore, in this work the voltage at the electrodes was set as a linear function of time,  $V(t)$ , with  $dV/dt = 1.3 \cdot 10^{15}$  V/s. The geometry used in the simulation represented a coaxial diode with 1-cm cathode-anode separation. The cathode was a needle with the tip radius  $r_c$  equal to several tens of micrometers. On the cathode surface there was a microprotrusion of height  $h_m$  (a few micrometers), tip radius  $r_m$ , and cone angle  $\Theta$  (see Fig. 1.). This cathode geometry takes into account the two-factor field enhancement at the microprotrusion surface which is typical of the electrode systems that were used in the experimental studies of EEE performed by now on the subnanosecond scale.

A two-dimensional two-temperature model which describes the processes of heat release due to surface and bulk sources, the energy exchange between the electron subsystem and phonons, and the heat transfer by electrons has been developed to investigate the prebreakdown phenomena in a cathode microprotrusion for the voltage pulse durations lying in the subnanosecond range. The thermal conductivity of the lattice, with the characteristic times of the problem  $< 10^{-11}$  s, is neglected.

The electric field potential  $u$  in the diode is calculated with the Poisson equation (1). The FEE current density  $j_{em}$  was assumed to depend on the self-consistent electric field at the microprotrusion surface in accordance with Miller–Good approximation (3)-(6). The electron  $T_e$  and phonon  $T_p$  temperature fields in the cathode are calculated with the heat conduction equations:

$$C_V^e \frac{\partial T_e}{\partial t} = \nabla(\lambda_e \nabla T_e) + \frac{j^2}{\sigma} - \mu_T j \nabla T_e - \alpha(T_e - T_p) \quad , \quad (7)$$

$$C_V^p \frac{\partial T_p}{\partial t} = \alpha(T_e - T_p) \quad , \quad (8)$$

where  $C_V^e$  and  $C_V^p$  are the specific heat of the electrons and phonons, respectively,  $\lambda_e$  is the electron thermal conductivity,  $\mu_T$  is the Thomson factor,  $\sigma$  is the electric conductivity,  $j$  is the current density in the cathode,  $\alpha$  is the energy exchange factor between the electron subsystem and phonons.

The boundary condition for equation (7, 8) is given by the resulting heat flux at the cathode surface:

$$-\lambda_e \nabla T_e|_S = q_N \quad , \quad \lambda_p \nabla T_p|_S = 0 \quad , \quad (9)$$

$$q_N = \frac{4\pi me}{h^3} \int_0^\infty \varepsilon \, d\varepsilon \int_0^\varepsilon d\varepsilon_n f_{FD}(\varepsilon) D(E_{em}, \varepsilon_n) - \frac{j_{em}}{e} \varepsilon_F \quad , \quad (10)$$

where  $q_N$  is the surface heat release due to Nottingham effect. The other boundary conditions are

$$\lambda_e \frac{\partial T_e}{\partial r} \Big|_s = 0, \text{ for } r=0, \quad r \rightarrow \infty, \quad (11)$$

$$T_e = T_p = T_0, \text{ for } z \rightarrow -\infty, \quad T_e(r, z) \Big|_{t=0} = T_p(r, z) \Big|_{t=0} = T_0, \quad (12)$$

where  $T_0 = 300$  K is the initial homogeneous temperature field for  $t = 0$ .

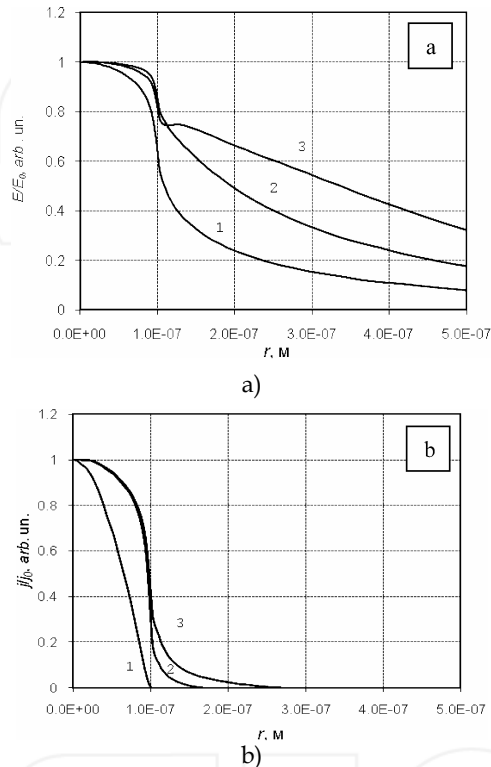


Fig. 12. Distributions of the electric field strength (a) and field emission current density (b) over the microprotrusion surface at different points in time: 1 -  $t = 2 \cdot 10^{-16}$  s,  $U = 20$  kV,  $T_0 = 300$  K,  $E_0 = 7.3 \cdot 10^7$  V/cm,  $j_0 = 4.5 \cdot 10^7$  A/cm<sup>2</sup>; 2 -  $t = 3.8 \cdot 10^{-11}$  s,  $U = 70.4$  kV,  $T_0 = 1300$  K,  $E_0 = 1.1 \cdot 10^8$  V/cm,  $j_0 = 1.0 \cdot 10^9$  A/cm<sup>2</sup>; 3 -  $t = 1.0 \cdot 10^{-10}$  s,  $U = 158$  kV,  $T_0 = 5300$  K,  $E_0 = 1.19 \cdot 10^8$  V/cm,  $j_0 = 3.2 \cdot 10^9$  A/cm<sup>2</sup>

The current density in the cathode  $\vec{j} = en_e v_e = (c / 4\pi) \text{rot} \vec{B}$  is determined through the magnetic induction equation:

$$\frac{\partial \vec{B}}{\partial t} = \text{rot} [\vec{v}_e \vec{B}] + \frac{c^2}{4\pi\sigma} \Delta \vec{B}. \quad (13)$$

Here,  $\vec{B}$  is the magnetic field,  $e$  is the electron charge,  $n_e$  is the electron density,  $v_e$  is the hydrodynamical velocity of the electrons,  $c$  is the light velocity.

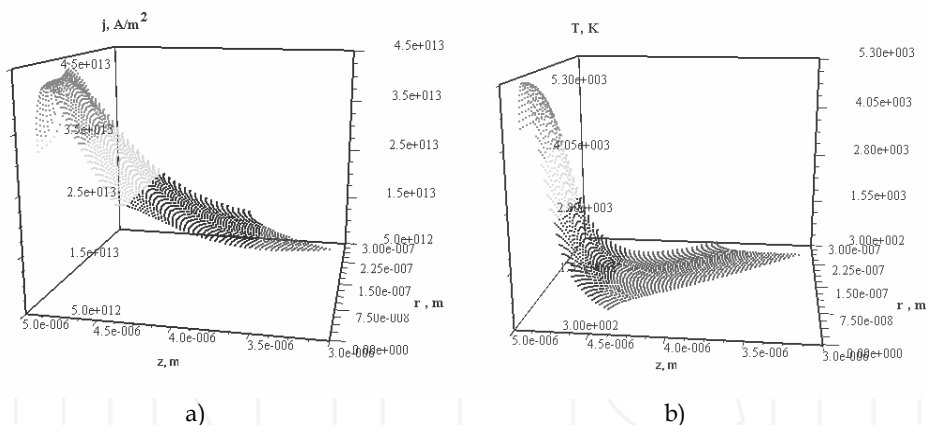


Fig. 13. Distributions of the current density (a) and electron temperature (b) in the Cu microprotrusion for  $t = 1.0 \cdot 10^{-10}$  s,  $U = 158$  kV,  $T_0 = 5300$  K,  $E_0 = 1.19 \cdot 10^8$  V/cm,  $j_0 = 3.2 \cdot 10^9$  A/cm<sup>2</sup>. Geometric parameters are given in Fig. 1

### 3.2 Results of numerical simulation

Figure 12 presents the distributions of the electric field strength and field emission current density over the microprotrusion surface at different points in time with a linearly increasing voltage at the electrodes for a copper cathode whose geometric parameters are given in Fig. 1. From Fig. 12 it can be seen that at  $j_0 > 10^9$  A/cm<sup>2</sup> the space charge substantially affects both the magnitude of the field and its distribution over the surface. Note that if the space charge would not been taken into account, the field distribution in Fig. 12 a would remain constant. Thus, the screening of the external field by the space charge of emitted electrons substantially levels off the electric field strength at the microprotrusion tip and, accordingly, increases the “effective emission area” (see Fig. 12 b).

With this current density distribution over the microprotrusion surface, the current density is enhanced, as illustrated in Fig. 13 a. Figure 13 b presents the temperature distribution of electrons at the microprotrusion for the same point in time.

The results of a simulation of the microprotrusion heating for different tip radii are given in Fig. 14. The time of relaxation of the lattice temperature  $\tau_T^p = C_V^p / \alpha$  and electron temperature  $\tau_T^e = C_V^e / \alpha$  are 48 ps and 0.3 ps, respectively. From Fig. 14 it can be seen that thermal instability of the microprotrusion within a time less than  $(1-2) \cdot 10^{-10}$  s can develop only for  $r_m < 0.1$   $\mu$ m. In this case, the difference in temperature between the electrons and the lattice can reach 0.5–1 eV. It should be noted that with the geometric parameters of the copper microprotrusion ( $r_m < 1$   $\mu$ m) and the parameters of the pulse used in this simulation ( $dV/dt = 1.3 \cdot 10^{15}$  V/s) the effect of a finite time of penetration of the magnetic field in the conductor (skin effect), which is responsible for the nonuniform current density distribution in the microprotrusion and, hence, for its nonuniform heating, is inappreciable. In order that this effect would qualitatively change the spatial distribution of bulk heat sources, shorter times of the processes involved are necessary.



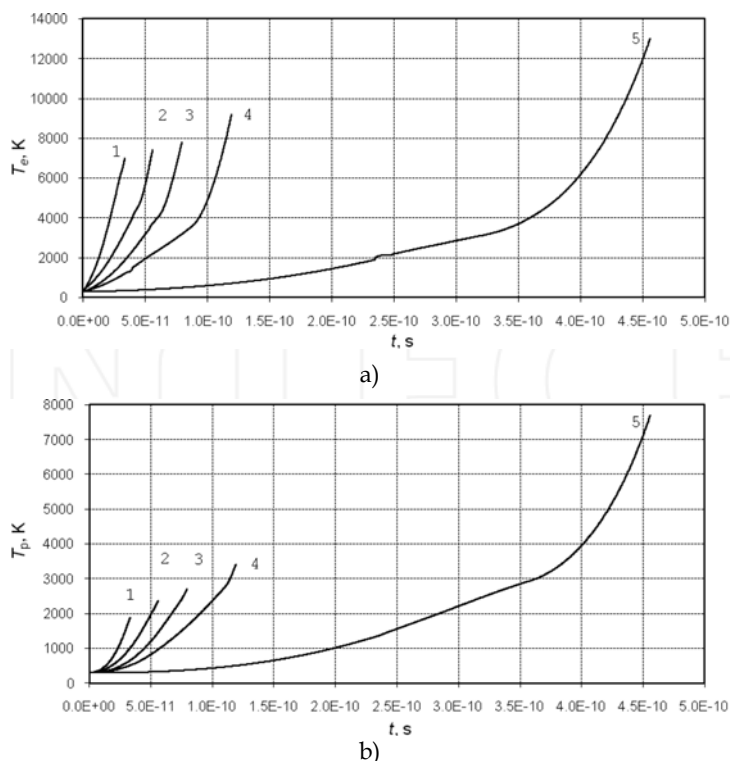


Fig. 14. Time dependences of the maximum electron temperature (a) and lattice temperature (b) in a microprotrusion for a copper cathode of different geometry with  $r_c = 50 \mu\text{m}$ ,  $h_m = 5 \mu\text{m}$ ,  $\Theta = 10 \text{ deg}$ , and  $r_m = 0.01 \mu\text{m}$  (1),  $0.03 \mu\text{m}$  (2),  $0.05 \mu\text{m}$  (3),  $0.1 \mu\text{m}$  (4), and  $0.5 \mu\text{m}$  (5).  $dU/dt = 1.3 \cdot 10^{15} \text{ V/s}$

#### 4. Initiation of an explosive center beneath the plasma of a vacuum arc cathode spot

Notwithstanding the fact that both the spark and the arc stage of vacuum discharges have been in wide practical use for many years, interest in developing theoretical ideas of the physical phenomena responsible for the operation of this type of discharge is being quickened. In common opinion, the most important and active region in a vacuum discharge is the cathode region. It is our belief that the most consistent and comprehensive model of a cathode spot is the ecton model (Mesyats, 2000). It is based on the recognition of the fundamental role of the microexplosions of cathode regions that give rise to explosive electron emission on a short time scale. The birth of such an explosive center – an ecton – is accompanied by the destruction of a cathode surface region, where a crater is then formed, the appearance of plasma in the electrode gap, and the formation of liquid-metal jets and droplets. An ecton, being an individual cell of a cathode spot, has a comparatively short lifetime (several tens of nanoseconds) (Mesyats, 2000). Therefore, an important issue in this theory is the appearance of new (secondary) explosive centers that would provide for the

self-sustaining of a vacuum discharge. According to (Mesyats, 2000), the most probable reason for the appearance of a new explosive center immediately in the zone of operation or in the vicinity of the previous one is the interaction of a dense plasma with the microprotrusions present on the cathode surface or with the liquid-metal jets ejected from the crater. These surface microprotrusions can be characterized by a parameter  $\beta_j$  which is equal to the ratio of the microprotrusion surface area to its base area and defines the current density enhancement factor. An investigation (Mesyats, 2000) of the development of the explosion of such microprotrusions in terms of the effect of enhancement of the current density of the ions moving from the plasma to the cathode and in view of the Joule mechanism of energy absorption has resulted in the conclusion that for an explosion to occur within  $10^{-9}$  s, it is necessary to have microprotrusions with  $\beta_j \geq 10^2$  at the ion current density  $\sim 10^7$  A·cm<sup>-2</sup>. This work is an extension of the mentioned model and describes the formation of secondary ectons upon the interaction of a dense plasma with cathode surface microprotrusions.

In the general case, the charge particle flow that closes onto a microprotrusion consists of three components: an ion flow and an electron flow from the plasma and a flow of emission electrons (Ecker, 1980; Hantzsche, 1995; Beilis, 1995). Each of these flows carries both an electric charge and an energy flux, forming a space charge zone at short distances from the cathode surface and giving rise to an electric field  $E_c$  at the cathode. In (He & Haug, 1997) the initiation of a cathode spot was investigated for the ion current  $j_i$  and the electric field at the cathode  $E_c$  specified arbitrarily from a "black box" and with an artificially created spatially homogeneous "plasma focus" of radius 10  $\mu$ m on a plane cathode. It has been shown that the cathode heating by incident ions and the enhancement of the electric field  $E_c$  by the ion space charge reduce the critical field at which the process of thermal run-away and overheating below the surface starts developing. It should however be noted that the least times of cathode spot initiation obtained in (He & Haug, 1997) are longer than 1  $\mu$ s. On the other hand, according to the ecton model of a cathode spot (Mesyats, 2000) and to the experimental data (see, for example (Juttner, 2001)), the cathode spot phenomena have an essentially nonstationary and cyclic character with the characteristic time scale ranging between  $10^{-9}$  and  $10^{-8}$  s.

Thus the goal of this section is to investigate the formation of secondary explosive centers upon the interaction of the plasma of a vacuum arc cathode spot with cathode surface microprotrusions (Uimanov, 2003).

#### 4.1 Description of the model of the Initiation of an explosive center

##### *The problem statement and task geometry*

Figure 15 presents the model geometry of the problem. The shape of the microprotrusion surface is specified by the Gauss function  $z_s = h \exp(-(r/d)^2)$ , where  $h$  is the height of the microprotrusion,  $d$  specifies the base radius  $r_m$  that is determined for  $z = 0.1h$ . We shall further characterize the geometry of a microprotrusion by a current density enhancement factor  $\beta_j = S / \pi r_m^2$ , where  $S$  is the surface area of the microprotrusion. In terms of this model, we assume that over the cathode surface there is a cathode spot plasma with an ion density  $n_i$  and an electron temperature  $T_e$  at the sheath edge. The quantities  $n_i$  and  $T_e$  are the problem parameters and, according to (Shmelev & Litvinov, 1998), they depend on the distance from the active explosive center.

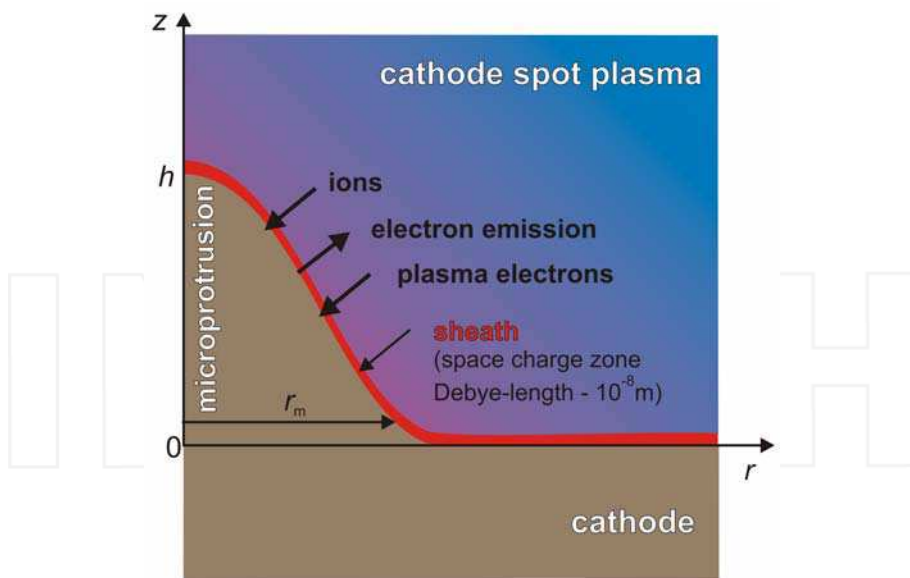


Fig. 15. Task geometry and a schematic description of the 2D model in a cylindrical symmetry

In view of the fact that the width of the space charge layer is much smaller than the characteristic dimensions of the microprotrusion, the layer parameters are considered in a one-dimensional (local) approximation.

*The temperature field*

The temperature field in the cathode is calculated with the heat conduction equation:

$$c_p \rho \frac{\partial T}{\partial t} = \frac{1}{r} \frac{\partial}{\partial r} \left( r \lambda \frac{\partial T}{\partial r} \right) + \frac{\partial}{\partial z} \left( \lambda \frac{\partial T}{\partial z} \right) + \frac{j^2}{\sigma}, \quad (14)$$

where  $c_p$  is the specific heat at constant pressure,  $\lambda$  is the thermal conductivity,  $\rho$  is the mass density,  $\sigma$  is the electric conductivity,  $j$  is the current density in the cathode. The parameters  $c_p$ ,  $\lambda$  and  $\sigma$  are considered as function of temperature  $T(r, z, t)$  (Zinoviev, 1989). The boundary condition for equation (14) is given by the resulting heat flux at the cathode surface:

$$-\lambda \nabla T|_s = q_s, \quad (15)$$

where  $q_s = q_N + q_i$  is the sum of the Nottingham effect  $q_N$  (see eq. 10) and ion impact heating  $q_i$  (evaporation cooling does not noticeably affect the final results). The other boundary conditions are

$$\lambda \frac{\partial T}{\partial r} = 0, \text{ for } r = 0, \quad r \rightarrow \infty, \quad T = T_0, \text{ for } z \rightarrow -\infty, \quad (16)$$

where  $T_0 = 300$  K is the initial homogeneous temperature field for  $t = 0$ .

### The Joule heating

The Ohm's electric potential  $U$  and current density  $\vec{j} = -\sigma \vec{\nabla} U$  in the cathode is determined through the continuity equation:

$$\frac{1}{r} \frac{\partial}{\partial r} \left( r \sigma \frac{\partial U}{\partial r} \right) + \frac{\partial}{\partial z} \left( \sigma \frac{\partial U}{\partial z} \right) = 0, \quad (17)$$

with boundary condition at the cathode surface:

$$-\nabla U|_s = j_s / \sigma. \quad (18)$$

Here  $j_s = j_{em} + j_i$  is the total current density at the cathode surface,  $j_{em}$  is the electron emission current density and  $j_i$  is the current density of the ions moving from the plasma to the cathode. The other boundary conditions are

$$\sigma \frac{\partial U}{\partial r} = 0, \text{ for } r=0, \quad r \rightarrow \infty, \quad U=0, \text{ for } z \rightarrow -\infty, \quad (19)$$

### The plasma-surface interaction

To calculate  $j_i$ , it is assumed that the ions are treated as monoenergetic particles, entering the sheath edge with Bohm's velocity and all ions recombine at the cathode surface. Then the expression for  $j_i$  can be written in the form:

$$j_i = Ze n_i \sqrt{\frac{kT_e}{m_i}}, \quad (20)$$

where  $Z$  is the mean ion charge,  $m_i$  is the ion mass. The power density input into the cathode surface from ion impact heating (Mesyats & Uimanov, 2006) is  $q_i = j_i \bar{U}$ , where  $Ze\bar{U} = ZeV_c + eV_i - Z\varepsilon_{em}$ . Here  $V_c$  is the cathode fall potential,  $V_i$  is the averaged ionization potential,  $\varepsilon_{em}$  is the averaged energy per emitted electron. The electron emission characteristics  $j_{em}$  and  $\varepsilon_{em} = q_N / (j_{em} / e)$  are calculated numerically in the MG approximation (see sec. 2.2 and sec. 3.1). Because of the high temperatures, the temperature drift of the chemical potential of the electron system inside the cathode is taken into account (see, for example (Klein et al., 1994)). To calculate the electric field at the cathode, the Mackeown-like equation is used, taking into account the electron flow from the spot plasma to the cathode (Mackeown, 1929; Mesyats & Uimanov, 2006; Beilis, 1995):

$$E_{em}^2 = \frac{4}{\varepsilon_0} \left[ j_i(n_i, T_e) \sqrt{\frac{m_i V_c}{2Ze}} \left\{ \sqrt{1 + \frac{kT_e}{2ZeV_c}} - \sqrt{\frac{kT_e}{2ZeV_c}} - \sqrt{\frac{kT_e}{2ZeV_c}} \left( 1 - \exp\left(-\frac{eV_c}{kT_e}\right) \right) \right\} - \right. \\ \left. - j_{em}(E_c, T_s) \sqrt{\frac{m_e V_c}{2e}} \right], \quad (21)$$

where  $T_s$  is the cathode surface temperature.

In conclusion of this section, we explain in more detail how the model proposed takes into account the contribution of the electron flow from the plasma to the cathode. If we assume

that the velocity distribution of the plasma electrons at the sheath edge is a Maxwellian one, we arrive at the statement that only the electrons whose velocities are higher than  $\sqrt{2eV_c/m_e}$  make a contribution to the current of the electrons 'counterdiffusing' from the quasineutral plasma to the cathode,  $j_{ep}$ . According to (Hantzsche, 1995), we have  $j_{ep} = -Zen_i\sqrt{kT_e/2\pi m_e}\exp(-eV_c/kT_e)$ . Then, in view of (20), the ratio of this contribution to the ion current density takes the form  $|j_{ep}|/j_i = \sqrt{m_i/2\pi m_e}\exp(-eV_c/kT_e)$ . For the parameters used in this work ( $\sqrt{m_i/m_e} \approx 340$ ,  $eV_c/kT_e = 8$ ), we have  $|j_{ep}|/j_i = 4.6 \cdot 10^{-2}$ . Therefore, in the boundary condition Eq. (18), we may neglect the contribution  $j_{ep}$  to the total current at the surface of the microprotrusion. The small ratio of the electron current to the current of the ions arriving at the cathode from the spot plasma permits us to ignore as well the energy flux density of these electrons,  $q_{ep}$ , in the general balance of the surface heat sources in the boundary condition Eq. (15). With the parameters used, we have  $q_{ep}/q_i \approx (0.1 \div 2) \times 10^{-2}$ . Thus, in the case under consideration, the contributions of  $j_{ep}$  and  $q_{ep}$  to the current and energy balance at the cathode surface can be neglected. At the same time, it should be stressed that the effect of the electron flow from the plasma to the cathode is essential in calculating the characteristics of the space charge sheath (see Eq. (21)). If we take account of the effect of the space charge of this flow, we obtain that  $E_c$  noticeably decreases. This results in a substantial change in the rate of the development of thermal instability because of the strong dependence of the emission characteristics on  $E_c$ .

Microprotrusion parameters					Explosion delay time $t_d$ , ns	
N	$h$ , $\mu\text{m}$	$d$ , $\mu\text{m}$	$r_{mv}$ , $\mu\text{m}$	$\beta_j$	$j_i = 5.6 \cdot 10^{10} \text{ A/m}^2$	$j_i = 1.1 \cdot 10^{11} \text{ A/m}^2$
1	0.5	0.312	0.5	1.4	-	10
2	1	0.312	0.5	2.2	-	1.5
3	1.5	0.312	0.5	3	16.3	0.8
4	1.75	0.312	0.5	3.52	5.2	0.71
5	2	0.312	0.5	4	3.55	0.68
6	3	0.312	0.5	5.9	2.26	0.57
7	5	0.312	0.5	9.74	1.5	0.33

Table 2. A set of geometrical parameters of the microprotrusions and the obtained explosion delay time

#### 4.2 Simulation of the microprotrusion heating

Computations were performed for a copper cathode with the following arc parameters:  $V_c = 16 \text{ V}$ ,  $eV_i = 18 \text{ eV}$ ,  $Z = 2$ . For the initial conditions of the problem, the characteristics of the plasma ( $n_i$ ,  $T_e$ ) at the sheath edge and the microprotrusion geometry ( $h$ ,  $d$ ) were specified. The computations were performed for a set of geometrical parameters of the microprotrusions, which are submitted in the Table 2.

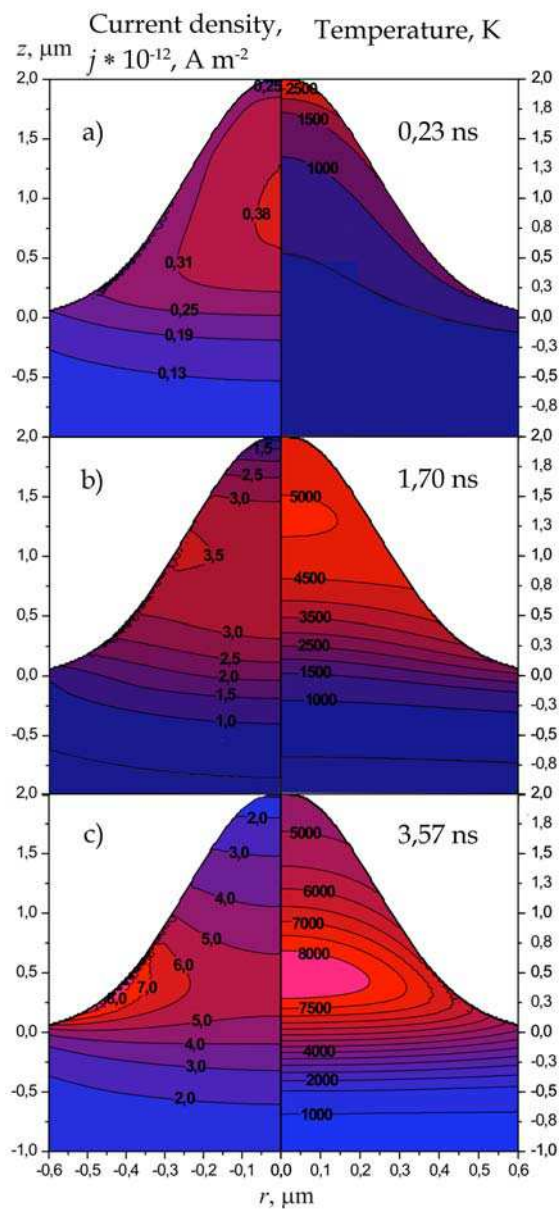


Fig. 16. Space distribution of temperature and current density modulus: a)  $t = 0.23 \text{ ns}$ , b)  $t = 1.9 \text{ ns}$ , c)  $t = 6.2 \text{ ns}$

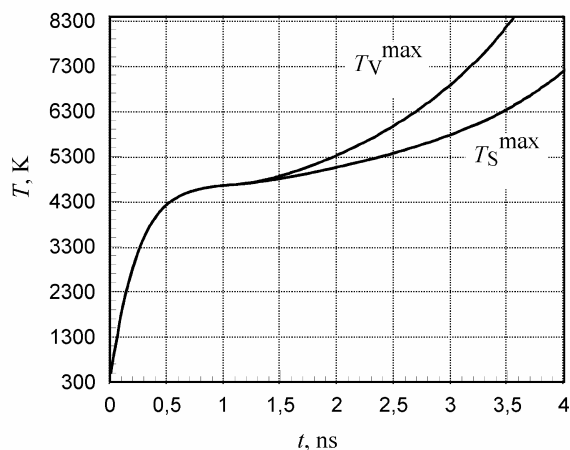


Fig. 17. The temperature evolution of the microprotrusion with  $\beta_j = 4$ . Cathode spot plasma parameters:  $n_i = 10^{26} \text{ m}^{-3}$   $T_e = 2 \text{ eV}$  ( $j_i = 5.6 \cdot 10^{10} \text{ A/m}^2$ ).  $T_S^{\max}$  is the surface maximum temperature and  $T_V^{\max}$  is the bulk maximum temperature that is reached below the surface due to emission cooling

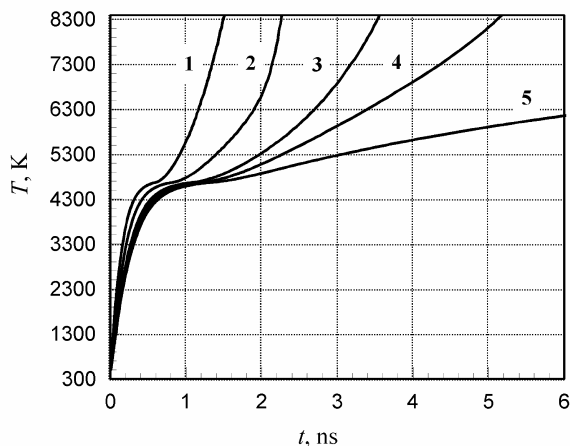


Fig. 18. The influence of the microprotrusion geometry on the initiation of the explosive stage: 1 -  $\beta_j = 9.74$ ; 2 -  $\beta_j = 5.9$ ; 3 -  $\beta_j = 4$ ; 4 -  $\beta_j = 3.52$ ; 5 -  $\beta_j = 3$ . Cathode spot plasma parameters:  $n_i = 10^{26} \text{ m}^{-3}$   $T_e = 2 \text{ eV}$  ( $j_i = 5.6 \cdot 10^{10} \text{ A/m}^2$ )

The computation is performed until the maximum temperature in the protrusion reaches a critical temperature  $T_{cr} = 8390 \text{ K}$ . As this happens, the model becomes inoperative, and the process goes to the explosive phase of the development of an ecton.

Figure 16 gives the results of computation for the temperature field and the spatial distribution of the current density modulus.

The simulation has shown that the heating of a microprotrusion can be subdivided by convention into two stages. At the first stage (see Fig. 16 a)), where the cathode is still comparatively cold, the surface heating due to ion impact prevails. In this case, the microprotrusion behaves as if it were a collecting thermal lens. The Joule heating at this stage was inessential. As the temperature reaches  $\sim 3500\text{--}4000\text{ K}$ , the emission current density increases substantially and intense surface cooling begins, and this can be associated with the onset of the second stage of heating (see Fig. 16 b)). At this point, the current density maximum is in the bulk of the microprotrusion and, hence, this is the region where intense Joule heat release begins. This region is responsible for the maximum temperature in the cathode at any subsequent point in time (see Fig. 16 c)). Then the maximum surface temperature shifting toward the protrusion base. The current density maximum also tends to move to this region since the current "makes attempts" to bypass the high-temperature region. After a time, this surface region has the highest surface temperature and emission current density. However, the most intense heat release occurs, as earlier, in the microprotrusion bulk, and thus a highly overheated region is formed which is surrounded by a not so hot surface. Figure 17 presents the time dependence of the temperature being a maximum throughout the microprotrusion and for the surface temperature that underlie the character of the above process of the heating of a microprotrusion.

Figure 18 was obtained with the same ion current density, but with different values for  $\beta_j$  (the microprotrusion geometry). It clearly shows the development of the thermal run-away regime and the initiation of the explosive stage.

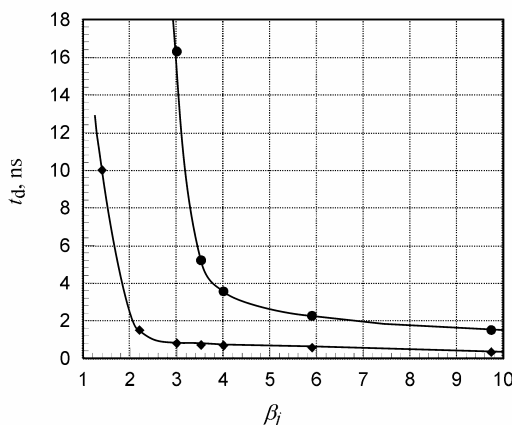


Fig. 19. Explosion delay time *vs* the current density enhancement factor  $\beta_j$  :  $\bullet$  -  $n_i = 10^{26} \text{ m}^{-3}$   $T_e = 2 \text{ eV}$  ( $j_i = 5.6 \cdot 10^{10} \text{ A/m}^2$ ),  $\blacklozenge$  -  $n_i = 1.8 \cdot 10^{26} \text{ m}^{-3}$   $T_e = 2 \text{ eV}$  ( $j_i = 1.1 \cdot 10^{11} \text{ A/m}^2$ )

The results of the computations performed are combined in Fig. 19 and Table 2 where the explosion delay time  $t_d$  (heating time from 300 K to  $T_{cr}$ ) is presented as a function of the microprotrusion geometry for a varied plasma density (ion current density).

It should be stressed that there is a range of comparatively small values of  $\beta_j$  where the given mechanism of the formation of secondary ectons can ensure the birth of new cathode spot cells upon the interaction of the plasma generated by active cells with cathode surface microprotrusions.



## 5. Conclusion

The effect of the space charge of the emitted electrons on the strength of the self-consistent electric field at the surface of a pointed microprotrusion and field emitter has been investigated for the first time in the framework of a two-dimensional axisymmetric statement of the problem. Based on the particles in cells method, a model has been developed and self-consistent calculations of the electric field and of the field emission characteristics of the copper cathode taking into account the space charge of emitted electrons have been performed for the range of emitter tip radius from  $\sim 10^{-4}$  cm to  $\sim 1$  nm. For the geometry under investigation it has been shown that the space-charge screening of the external field is substantially less pronounced for emitters whose tip radii are comparable to the size of the region where the space charge is mostly localized. As for emitters having nanometer tip radii, their CVCs remain linear in the F-N coordinates up to FEE current densities of  $\sim 10^9$  A/cm<sup>2</sup>. Despite the significant screening of the external field at high FEE current densities, the emission current density for microprotrusions with tip radii  $r_m < 0.1$   $\mu$ m can reach  $\sim 10^{10}$  A/cm<sup>2</sup>. Based on the criterion for pulsed breakdown (Mesyats, 2000), it can be shown that, in view of Joule heating, this current density suffices for the FEE-to-EEE transition to occur within less than  $10^{-10}$  s.

A two-dimensional, two-temperature model has been developed to describe the prebreakdown phenomena in a cathode microprotrusion at nanosecond durations of the applied voltage pulse. The simulation procedure includes (i) a particle-in-cell simulation to calculate the self-consistent electric field at the cathode and the field-emission characteristics of the cathode; (ii) calculations of the current density distribution in the cathode microprotrusion in view of a finite time of electromagnetic field penetration in the conductor; (iii) calculations of the electron temperature based on the heat equation taking into account volumetric (Joule-Thomson effect) and surface (Nottingham effect) heat sources, and (iv) calculations of the lattice temperature based on the heat equation taking into account the finite time of electron-phonon collisions. A numerical simulation performed for a copper cathode for voltage pulses with  $\sim 10^{15}$  V/s rise rates has demonstrated that (i) the screening of the external field by the space charge of emitted electrons has the result that the electric field strength levels off approaching to that at the microprotrusion tip, and this gives rise to a region inside the microprotrusion where the current density is about twice the maximum field emission current density at the tip; (ii) the electron temperature can be greater than the lattice temperature by 0.5–1 eV at the onset of the explosive metal-plasma phase transition; (iii) with a 5- $\mu$ m characteristic height of microprotrusions on a point cathode whose radius of curvature is 50  $\mu$ m the field emission-to-explosive emission transition can occur within 100–200 ps only for microprotrusions with a tip radius no more than 0.1  $\mu$ m.

A two-dimensional nonstationary model of the initiation of new explosive centers beneath the plasma of a vacuum arc cathode spot has been developed. In terms of this model, the plasma density and electron temperature that determine the ion current from the plasma to the microprotrusion and the microprotrusion geometry were treated as the external parameters of the problem. The process of heating of a cathode surface microprotrusion, for which both a surface irregularity resulting from the development of a preceding crater and the edge of an active crater, which may be a liquid-metal jet, can be considered, has been simulated numerically. Based on the computation results, one can make the following conclusions:

- i. The heating of a microprotrusion gives rise to a strongly overheated region in the protrusion bulk. Hence, an expansion of such a microregion of the cathode, being in an extreme state, should be explosive in character.
- ii. Taking into account the ion impact heating and the electric field of the space charge layer near the cathode surface ensure the "triggering" heat flux power necessary for the development of the Joule heating of the microprotrusion followed by its explosion at reasonable values of the ion current ( $j_i < 10^7 \text{ A}\cdot\text{cm}^{-2}$ ) and of the geometric parameters of the microprotrusion ( $\beta_j < 10$ ).

## 6. Acknowledgment

The author would like to thank Academician G. A. Mesyats, who provided encouragement and stimulating discussion.

The work was partially supported by the Russian Fundamental Research Foundation under Awards 10-08-00517, 08-02-00720 and the integration project of the Presidium UB RAS No. 09-C-2-10002.

## 7. References

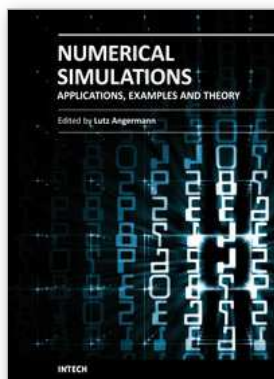
- Barbour, J.P.; Do1an, W.W.; Tro1an, J.K.; Martin, E.E. & Dyke, W.P. (1963). *Phys. Rev.*, Vol. 92, (1963), p. 45
- Batratkov, A.V.; Pegel, I.V. & Proskurovsky, D.I. (1999). On the screening of the electric field at the cathode surface by an electron space charge at intense field emission, *IEEE Trans. Dielectrics El.*, Vol. 6, No. 4, August 1999, pp. 436-440, ISSN 1070-9878
- Batratkov, A.V.; Pegel, I.V. & Proskurovsky, D.I. (1999). *Rus. Pisma J. Tech. Physics*, Vol. 25, (1999), p. 78
- Beilis, I.I. (1995). Theoretical Modeling of Cathode Spot Phenomena, In: *Handbook of Vacuum Arc Science and Technology*, Boxman, R.L. et. al. (Ed.), pp. 208-256, Noyes, New Jersey
- Birdsall, C.K. & Langdon, A.B. (1985). *Plasma Physics, via Computer Simulation*, McGraw-Hill Book Company
- Dyke, W.P. & Trolan, J.K. (1953). *Phys. Rev.*, Vol. 89, (1953), p. 799
- Dyke, W.P.; Tro1an, J.K.; Do1an, W.W. & Barbour, J.P. (1953). *J. Appl. Phys.*, Vol. 24, p. 570
- Ecker, G. (1980). Theoretical aspects of the vacuum arc, In: *Theory and Application*, Lafferty, J.M. (Ed.), pp.228-320, Wiley, New York
- Forbes, R.G. (2001). *Sol. St. Electron*, Vol. 45, (2001), p. 779
- Fursey, G.N.; Baskin, L.M.; Glasanov, D.V. et al. (1998). *J. Vac. Sci. Technol. B*, Vol. 16, (1998), p. 232
- Fowler, R.H. & Nordheim, L. (1928). *Proc. Roy. Soc.*, Vol. 119, (1928), p. 173
- Guillorn, M.A.; Yang, X.; Melechko, A.V. et al. (2004). *J. Vac. Sci. Technol. B*, Vol. 22, (2004), p. 35
- Handbook of Vacuum Arc Science and Technology* (1995). Boxman, R.L.; Martin, P.J. & Sanders, D.M. (Ed.), Noyes Publications, Park Ridge
- Hantzsch, E. (1995). Theories of Cathode Spots In: *Handbook of Vacuum Arc Science and Technology*, Boxman, R.L. et. al. (Ed.), pp.151-208, Noyes, New Jersey

- He, Z.-J. & Haug, R. (1997). Cathode spot initiation in different external conditions, *J. Phys. D: Appl. Phys.*, Vol. 30, No. 4, Feb. 1997, pp. 603-613
- Hockney, R.W. & Eastwood, J.W. (1988). *Computer Simulation Using Particles*, IOP Publishing, Bristol
- Juttner, B. (2001). Cathode spots of electric arcs, *J. Phys. D: Appl. Phys.*, Vol. 34, No. 17, Sep. 2001, pp. R103-R123
- Klein, T.; Paulini, J. & Simon, G. (1994). Time-resolved description of cathode spot development in vacuum arcs, *J. Phys. D: Appl. Phys.*, Vol. 27, No. 9, Sep. 1994, pp. 1914-1921
- Lyubimov, G.A. & Rakhovskii, B.I. (1978). The cathode spot of a vacuum arc, *Physics-Uspeski*, Vol. 21, pp. 693-718
- Mackeown, S.S. (1929). The Cathode Drop in an Electric Arc, *Phys. Rev.*, Vol. 34, No. 4, Aug. 1929, pp. 611-614
- Mesyats, G.A. & Uimanov, I.V. (2006). On the limiting density of field emission current from metals, *IEEE Trans. Dielect. Elec. Insul.*, Vol. 13, (Feb. 2006), pp. 105-110
- Mesyats, G.A. & Uimanov, I.V. (2008). Numerical Simulation of Vacuum Prebreakdown Phenomena in a Cathode Microprotrusion at Subnanosecond Pulse Durations, *Proc. of XVIIIth Int. Symp. On Disch. and Electr. Insul. in Vac.*, pp. 17-20, ISBN 978-973-755-382-9, Bucharest, Romania, Sept. 2008, MATRIX ROM, Bucharest
- Mesyats, G.A. & Yalandin, M.I. (2005). High-power picosecond electronics, *Physics-Uspeski*, Vol. 48, No. 3, Mar. 2005, pp. 211-229
- Mesyats, G.A. (2000). *Cathode Phenomena in Vacuum Discharge: the Breakdown, the Spark and the Arc*, Nauka Publisher, ISBN 5-02-022567-3, Moscow
- Modinos, A. (1984). *Field, Thermionic and Secondary Electron Emission Spectroscopy*. Plenum Press, New York
- Nordheim, L. (1929). *Physikalische Zeitschrift*, Vol. 30, (1929), p. 117
- Pavlov, V.G. (2004). *Rus. J. Tech. Physics*, Vol. 74, (2004), p. 72
- Pavlov, V.G.; Rabinovich, A.A. & Shrednik, V.N. (1975). *Rus. J. Tech. Physics*, Vol. 45, (1975), p. 2126
- Seldner, D. & Westermann, T. (1988). Algorithms for Interpolation and Localization in Irregular 2D Meshes, *J. of Comp. Phys.*, Vol. 79, (Nov. 1988), pp. 1-11
- Shkuratov, S.I.; Barengolts, S.A. & Litvinov, E.A. (1995). Heating and Failure of Niobium Tip Cathode due to a High-density Pulsed Field Electron Emission Current, *J. Vac. Sci. Technol. B*, Vol. B13, No. 5, 1995, pp. 1960-1967
- Shmelev, D.L. & Litvinov, E.A. (1998). Computer simulation of ecton in vacuum arc, *IEEE Trans. Dielectrics El.*, Vol. 6, No. 4, August 1999, pp. 441-444, ISSN 1070-9878
- Shrednik, V.N. (1974). In: *Cold Cathodes*, pp. 165-190, Sov. Radio, Moscow
- Spindt, C.A. (1968). *J. Appl. Phys.*, Vol. 39, (1968), p. 3504
- Stern, T.E.; Gosling, B.S. & Fowler R.H. (1929). *Roy. Soc. Proc.*, Vol. A 124, (1929), p. 699
- Uimanov, I.V. (2003). A Two-Dimensional Nonstationary Model Of The Initiation Of An Explosive Center Beneath The Plasma Of A Vacuum Arc Cathode Spot, *IEEE Transaction on Plasma Science*, Vol. 31, N. 5, 2003, pp. 822-826
- Uimanov, I.V. (2008). PIC Simulation of the Electric Field at a Cathode with a Surface Microprotrusion Under Intense Field Emission, *Proc. of XVIIIth Int. Symp. On Disch. and Electr. Insul. in Vac.*, pp. 29-31, Bucharest, Romania, (2008)

- Uimanov, I.V. (2010). The Dimensional Effect of the Space Charge of the Emitted Electrons on the Strength of the Self-consistent Electric Field at the Cathode Surface, *Proc. 16th International Symposium on High Current Electronics*, Tomsk, Russia (to be published) (2010)
- Zinoviev, V.E. (1989). *Thermal Properties of Metals at High Temperatures. Reference Book.* Metallurgia, Moscow

INTECH

INTECH



## **Numerical Simulations - Applications, Examples and Theory**

Edited by Prof. Lutz Angermann

ISBN 978-953-307-440-5

Hard cover, 520 pages

**Publisher** InTech

**Published online** 30, January, 2011

**Published in print edition** January, 2011

This book will interest researchers, scientists, engineers and graduate students in many disciplines, who make use of mathematical modeling and computer simulation. Although it represents only a small sample of the research activity on numerical simulations, the book will certainly serve as a valuable tool for researchers interested in getting involved in this multidisciplinary field. It will be useful to encourage further experimental and theoretical researches in the above mentioned areas of numerical simulation.

### **How to reference**

In order to correctly reference this scholarly work, feel free to copy and paste the following:

Igor Uimanov (2011). Numerical Simulation of the Fast Processes in a Vacuum Electrical Discharge, Numerical Simulations - Applications, Examples and Theory, Prof. Lutz Angermann (Ed.), ISBN: 978-953-307-440-5, InTech, Available from: <http://www.intechopen.com/books/numerical-simulations-applications-examples-and-theory/numerical-simulation-of-the-fast-processes-in-a-vacuum-electrical-discharge>

**INTeCH**  
open science | open minds

### **InTech Europe**

University Campus STeP Ri  
Slavka Krautzeka 83/A  
51000 Rijeka, Croatia  
Phone: +385 (51) 770 447  
Fax: +385 (51) 686 166  
[www.intechopen.com](http://www.intechopen.com)

### **InTech China**

Unit 405, Office Block, Hotel Equatorial Shanghai  
No.65, Yan An Road (West), Shanghai, 200040, China  
中国上海市延安西路65号上海国际贵都大饭店办公楼405单元  
Phone: +86-21-62489820  
Fax: +86-21-62489821